Full-length RNA transcript sequencing traces brain isoform diversity in house mouse natural populations

Wenyu Zhang[1,2,3*], Anja Guenther[3,4], Yuanxiao Gao[5], Kristian Ullrich[3], Bruno Huettel[6], Aftab Ahmad[1], Lei Duan[1], Kaizong Wei[1] and Diethard Tautz[3,*]

[1] Shaanxi Key Laboratory of Qinling Ecological Intelligent Monitoring and Protection, School of Ecology and Environment, Northwestern Polytechnical University, Xi'an 710129, China

[2] Research & Development Institute of Northwestern Polytechnical University in Shenzhen, Shenzhen 518063, China

[3] Department of Evolutionary Genetics, Max Planck Institute for Evolutionary Biology, Ploen 24306, Germany

[4] Research Group Behavioral Ecology of Individual Differences, Max Planck Institute for Evolutionary Biology, Ploen, 24306, Germany

[5] School of Mathematics & Data Science, Shaanxi University of Science & Technology, Xi'an 710021, China

[6] Max-Planck-Genome-Centre Cologne, MPI for Plant Breeding Research, Cologne 50829, Germany

***Corresponding authors:**

Wenyu Zhang; Phone: +86 029-8843-1769; E-mail: wyzhang@nwpu.edu.cn

Diethard Tautz; Phone: +49 4522-763-390; E-mail: tautz@evolbio.mpg.de

Running title: Isoform diversity in house mouse natural populations

Manuscript type: Resource

Abstract

The ability to generate multiple RNA transcript isoforms from the same gene is a general phenomenon in eukaryotes. However, the complexity and diversity of alternative isoforms in natural populations remain largely unexplored. Using a newly developed full-length transcripts enrichment protocol with 5' CAP selection, we sequenced full-length RNA transcripts of 48 individuals from outbred populations and subspecies of *Mus musculus*, and from the closely related sister species *Mus spretus* and *Mus spicilegus* as outgroups. The dataset represents the most extensive full-length high-quality isoform catalog at the population level to date. In total, we reliably identified 117,728 distinct isoforms, of which only 51% were previously annotated. We show that the population-specific distribution pattern of isoforms is phylogenetically informative and reflects the segregating SNP diversity between the populations. We find that ancient housekeeping genes are a major source of the overall isoform diversity, and that the generation of alternative first exons plays a major role in generating new isoforms. Given that our data allow us to distinguish between population-specific isoforms and isoforms that are conserved across multiple populations, it is possible to refine the annotation of the reference mouse genome to a set of about 40,000 isoforms that should be most relevant for comparative functional analysis across species.

Keywords

Isoform diversity, full-length transcript sequencing, CAP selection, house mouse natural populations, LRS Special Issue

Introduction

The ability to generate multiple RNA isoforms from the same gene increases vastly the complexity of the transcriptome and proteome in eukaryotes (Keren et al. 2010; Nilsen and Graveley 2010). Alternative isoforms with different coding sequences can be generated through multiple types of alternative splicing events (Naftaly et al. 2021), including skipped exon (SE), retained intron (RI), mutually exclusive exons (MX), alternative 5' (A5'), and 3' (A3') splice sites. Isoform diversity can also be expanded via the inclusion of alternative transcription start sites (TSSs) or transcript end sites (TESs), resulting in differences in the untranslated regions (UTRs) (Landry et al. 2003; Tian and Manley 2017).

By analyzing high-throughput EST and short-read RNA-Seq data across species, several comparative studies on the complexity of isoform landscape have been performed in plants (Ling et al. 2019), insects (Malko et al. 2006), vertebrates (Mudge et al. 2011; Barbosa-Morais et al. 2012), birds (Rogers et al. 2021), mice (Harr and Turner 2010), and primates (Lin et al. 2010). These initial comparative studies have provided important insights into the enormous diversity of alternative isoforms, but only at the local level of splicing junction events due to the limitation of the short-read sequencing technology.

The recent development of long-read single-molecule sequencing technologies has enabled the capture of the full-length isoform diversity (Byrne et al. 2019), further facilitating the comparative analysis of alternative isoforms in different species. Leung SK et al. (Leung et al. 2021) used long-read isoform sequencing to generate full-length transcript sequences in the human and mouse cortex. They showed a similar global pattern of isoform diversity between humans and mice but with striking differences in some

genes between these two species. Another recent study from Ferrandez-Peral L (Ferrandez-Peral et al. 2022) generated an extensive full-length isoform catalog in primates and found that a high isoform diversity in immune genes correlates with signals of positive selection in the coding regions of the genes. These between-species comparison studies have provided insights into the complexity of alternative isoforms at a deep evolutionary time scale. However, the diversity and pattern of the alternative isoform landscape within natural populations remain largely unexplored (Verta and Jacobs 2022).

Owing to its well-defined evolutionary history (Guenet and Bonhomme 2003; Phifer-Rixey and Nachman 2015), the house mouse (*Mus musculus*) is a particularly suitable model system for studying the dynamics of polymorphisms and recently originated genetic elements in natural populations. Currently, three major lineages of the house mouse, which diverged roughly half a million years ago, are distinguished as subspecies (Harr et al. 2016): the Western European house mouse *Mus musculus domesticus*, the Eastern European house mouse *Mus musculus musculus*, and the Southeast Asian house mouse *Mus musculus castaneus.* With a divergence time of fewer than 2 million years, closely related outgroup species (*e.g.*, *Mus spretus*) are also available in this model system (Harr et al. 2016). We have previously used the house mouse system to study the evolutionary pattern of single nucleotide variants (Staubach et al. 2012), gene copy number variants (Pezer et al. 2015), and gene retrocopy variants (Zhang et al. 2021; Zhang and Tautz 2022). This made the house mouse an ideal system to directly trace the origin and pattern of alternative isoforms in natural populations.

Here, we use mice brains as the source tissue for the transcriptome analysis. The brain harbors the largest diversity of cell types with an overall transcript diversity only comparable to testis (Bekpen et al. 2018), but with many more of these transcripts being likely to be functional in the brain compared to the testis, where there is a lot of expression due to a transcriptionally permissive chromatin environment, especially in late spermatogenic cell types (Murat et al. 2023). Previous studies have made use of long-read sequencing to discover the isoform diversities in cell types and developmental stages of the laboratory mouse inbred strain C57Bl6 (Gupta et al. 2018; Lebrigand et al. 2020; Joglekar et al. 2021; Ding et al. 2022). However, the brain isoform diversity in wild mice, especially across natural populations, has so far only been studied at the short-read level (Harr and Turner 2010).

In the present study, we explore the brain isoform diversity in house moue natural populations and closely related outgroup species. Using an optimized protocol to capture predominantly full-length capped transcripts, we identify widespread brain isoform diversity. We assess whether the individual isoform landscape can be used to trace the differentiation history of house mouse natural populations. We further analyze the origin of the isoform diversity and explore the possible source of genes and local alternative splicing events that contribute most to the overall isoform diversity. With the newly generated comprehensive transcriptomic data, we aim to define the set of conserved isoforms across mouse species, which are of particular relevance for functional studies that use the mouse as a biomedical model system in comparison to humans.

Results

An optimized experimental protocol to enrich full-length transcript

A key step for full-length RNA sequencing is the enrichment of intact transcripts without degradation, ideally with hallmarks of both, a 5' CAP and a poly(A) tail. It has been reported that the TeloPrime full-length cDNA Amplification kit could selectively synthesize cDNA molecules from mRNAs carrying a 5' CAP, in complement to the standard PacBio cDNA library preparation protocol that could only selectively synthesize cDNA molecules from transcripts with a poly(A) tail (Cartolano et al. 2016). In this study, we developed a new PacBio Iso-Seq library preparation protocol via combining 5'CAP capture in the TeloPrime full-length cDNA Amplification kit and poly(A) tail enrichment in the standard PacBio cDNA synthesis kit, which can synthesize cDNA molecules from transcripts with both a 5' CAP and a poly(A) tail.

To test the performance of the TeloPrime-based protocol in an actual sample, we selected one mouse individual from the Taiwan population (Supplemental Data S1A) and implemented three distinct cDNA library preparation protocols for the RNA samples extracted from the brain (Figure 1A): i) standard PacBio cDNA library preparation protocol; ii) TeloPrime-based protocol with cDNA Amplification Kit v1; iii) TeloPrime-based protocol with cDNA Amplification Kit v2. The TeloPrime-based kit v2 includes updated reaction conditions compared to kit v1, while the method of cDNA generation remains unchanged. Each of the three cDNA libraries was sequenced on one SMRT cell of the same sequencing run, and the sequencing reads were analyzed and compared using the same computational approach (see Methods). Comparably high numbers of CCS reads were generated from each SMRT cell of the three kits (Supplemental Data S1A, Clontech: 472 k; Teloprime v1: 424 k; Teloprime v2: 437 k), ensuring the equivalent high-quality of these SMRT cells.

As shown in Figure 1B, we found that the sub-reads generated from TeloPrime-based cDNA libraries are, on average, longer (TeloPrime v1: 1,467bp; TeloPrime v2: 1,459bp) compared with those from the standard Clontech cDNA library (mean value: 1,085bp). Compared with that from the Clontech cDNA library (32.6%), a much higher fraction of isoforms from the TeloPrime v1 cDNA library (56.5%) and TeloPrime v2 cDNA library (57.3%) showed a complete and exact match of the exon chain as the annotated reference transcripts (Figure 1C and 1D). Moreover, around 50% of the isoforms from the Clontech cDNA library showed truncation of terminal exons. In comparison, this value is only 15.9% in the TeloPrime v1 cDNA library and 14.7% in the TeloPrime v2 cDNA library, suggesting that the TeloPrime-based cDNA enrichment protocols are more likely to enrich full-length transcripts. An in-depth investigation of the truncation lengths showed that the isoforms from the Clontech cDNA library are actually at least 2-fold more severely truncated from 5'end than those from TeloPrime-based cDNA libraries (similarly less extent from 3'end, Figure 1E), which confirmed the reliability of TeloPrime-based cDNA kits to selectively enrich mRNA transcripts carrying a 5' CAP (Cartolano et al. 2016). Analysis of the 5′-exons of isoforms that were truncated in the Clontech kit showed that the 5' terminal exons of the references transcripts tended to be longer (Supplemental Figure S1B) and more structured in an overall RNA structure analysis (Supplemental Figure S1C), both factors that may have contributed to the truncation tendency.

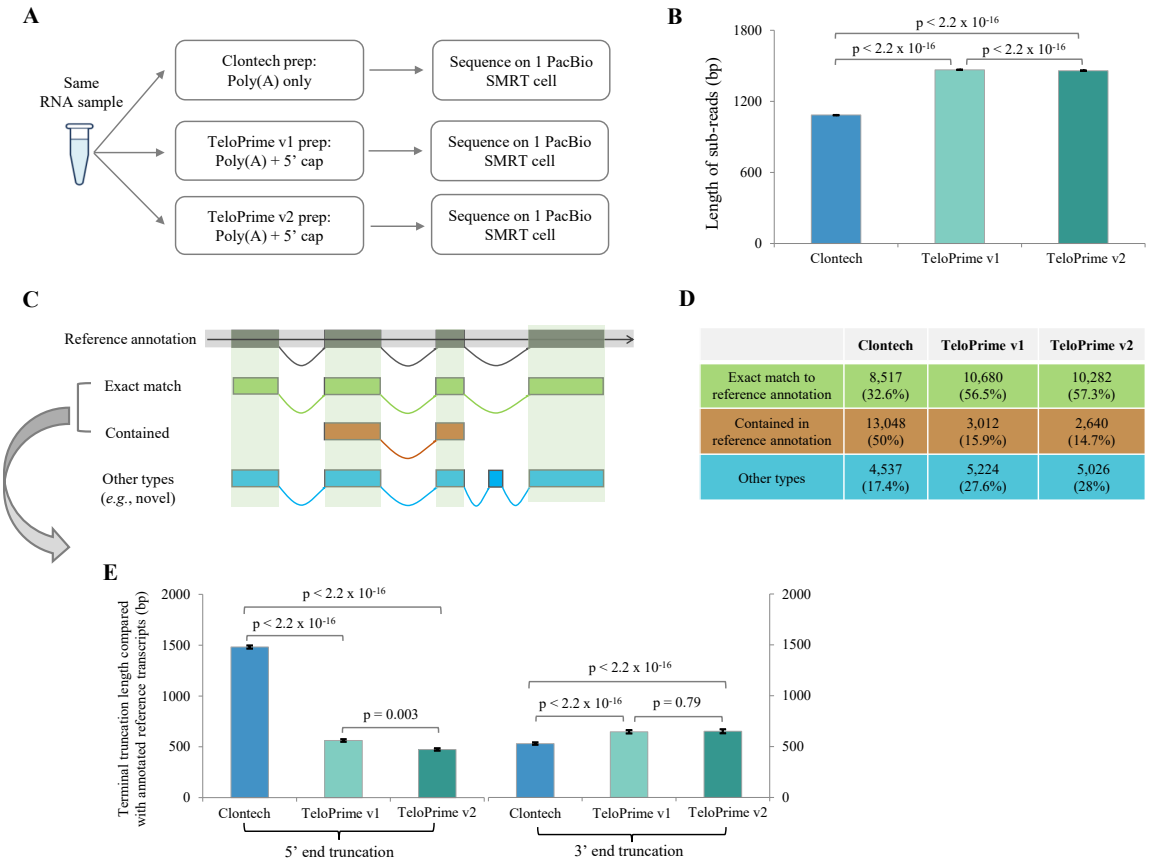

	Clontech	TeloPrime v1	TeloPrime v2
Exact match to reference annotation	8,517 (32.6%)	10,680 (56.5%)	10,282 (57.3%)
Contained in reference annotation	13,048 (50%)	3,012 (15.9%)	2,640 (14.7%)
Other types	4,537 (17.4%)	5,224 (27.6%)	5,026 (28%)

Figure 1 Performance evaluation of three types of full-length transcript enrichment protocols. (A) shows a simplified flow chart of this evaluation experiment setup. (B) indicates the length distribution of sub-reads generated from three PacBio Iso-Seq libraries. (C) illustrates the major categories of Iso-Seq transcripts based on their alignment coordinates to the reference genome, and (D) for the distribution of these categories. (E) shows the terminal truncation length of Iso-Seq transcripts from both 5' and 3' ends, compared to the reference annotation in Ensembl v103. Only Iso-Seq transcripts with exact matches or wholly contained in reference annotation were taken for analysis. The error bars indicate the standard error of means (SEM) of the length values. Statistical p-values were computed using two-sided Wilcoxon rank sum tests.

These findings suggest that the newly developed TeloPrime-based protocol provides a better approach to enriching full-length transcripts. Given the optimized reaction conditions, including the selection for capped RNA, we applied the TeloPrime-based protocol with cDNA Amplification Kit v2 to generate cDNA libraries for PacBio Iso-Seq for the following analyses.

Alternative isoform landscape in wild mice brains

We analyzed the isoform landscape in whole brain transcriptomes for forty-eight unrelated outbred wild-type mice individuals raised under tightly controlled laboratory conditions (Supplemental Data S1B). They

157 included forty house mouse (*Mus musculus*) individuals derived from five natural populations in the three
158 major subspecies (*M. m. domesticus*, *M. m. musculus*, and *M. m. castaneus*), as well as eight individuals
159 from two closely related outgroup species (*Mus spicilegus* and *Mus spretus*) (geographical origins and
160 evolutionary relationships are depicted in Figure 2A). We performed both PacBio Iso-Seq and Illumina
161 RNA-Seq for each brain sample to generate high-quality transcriptomes. As a result, an average of 60.1 (SD:
162 9.6) million raw sub-reads and 28.2 (SD: 3.3) million raw read pairs per sample were produced for PacBio
163 Iso-Seq and Illumina RNA-Seq, respectively (Supplemental Table S1). This dataset represents the largest
164 full-length isoform category at a comparative population level to date.

165 An overview of the methodology to generate the high-quality transcriptome is given in Supplemental Figure
166 S2. In brief, the raw PacBio Iso-Seq subread data were processed to produce circular consensus sequences
167 (CCS) and further refined to generate full-length non-chimeric (FLNC) reads using the IsoSeq3 pipeline.
168 To identify high-confidence isoforms, the FLNC reads were subject to *de novo* clustering using the same
169 IsoSeq3 pipeline to generate an average of 49,147 (SD: 4,554) non-redundant isoforms per sample
170 (Supplemental Data S1B), with the support from at least two FLNC reads (see below for the justification of
171 this cutoff). We aligned the unique isoforms of each sample to the GRCm39/mm39 reference genome using
172 minimap2 (Li 2018) and used the TAMA program (Kuo et al. 2020) with optimized parameters
173 (Supplemental Text of Methods and Supplemental Figure S3) to collapse and merge the transcript models
174 across all 48 samples into a single non-redundant transcriptome. We further refined a computational pipeline
175 to filter out low-quality transcripts and those of potential artifacts (see Methods), resulting in a total of
176 117,728 high-confidence distinct isoforms derived from 15,012 distinct loci (Supplemental Data S2). For
177 reference, we also include the list of isoforms covered only by singleton reads (Supplemental Data S3), but
178 we do not include these in the further analyses.

179 To evaluate the reliability of these isoforms, we assessed their quality for three distinct criteria separately:
180 i) transcription start site (TSS), ii) transcript end site (TES), and iii) splice junctions (SJ). Reliable TSSs are
181 defined as those supported by Ensembl GRCm39/mm39 reference genome annotation (Howe et al. 2021),
182 collection of experimentally validated TSS peaks (Abugessaisa et al. 2019), and a significantly greater
183 coverage ratio between inside isoform and outside isoform than the null hypothesis (Tardaguila et al. 2018)
184 (Supplemental Figure S4). Similarly, reliable TESs are defined as those supported by the reference genome
185 annotation (Howe et al. 2021) and collection of experimentally validated poly(A) sites and motifs
186 (Herrmann et al. 2020). The reliable SJs are defined as those present in reference genome annotation (Howe
187 et al. 2021) and those belonging to the canonical splicing signals (GT-AG, GC-AG, and AT-AC) (Parada et
188 al. 2014). A more detailed discussion on evaluating the reliability of the detected isoforms can be found in
189 the Supplemental Text of Methods, including Supplemental Figures S5 and S6. Based on the above-defined
190 criteria, we found that 98.7% of the TSSs, 94.4% of the TESs, and 99.1% of the SJs from all the detected
191 isoforms are supported by respective previous evidence (Supplemental Data S2), and a comparable large
192 extent (>96% for all three features) of isoforms could be validated for all the seven tested populations
193 (Supplemental Figure S7).

194

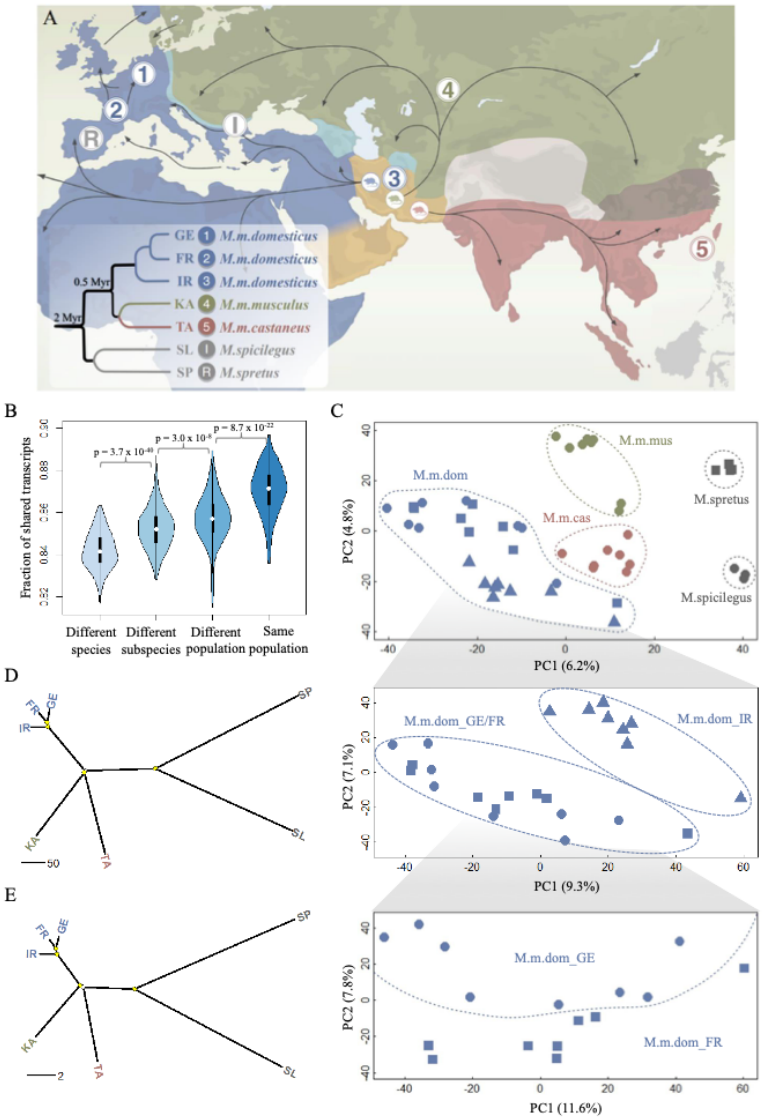

Figure 2 Geographic locations and phylogenetic relations of sampled mice individuals. (A) Geographic locations for the sampled mouse populations in this study. Territory areas for each house mouse subspecies: *M. m. domesticus* (blue), *M. m. musculus* (green), and *M. m. castaneus* (brown). Black arrows indicate possible migration routes, mainly during the spread of agriculture and trading. The inset figure shows the canonical phylogenetic relationships among the house mouse populations and outgroup species (branch lengths not scaled)**.** Geographic locations: 1, Germany (GE); 2, France (FR); 3, Iran (IR); 4, Kazakhstan (KA); 5, Taiwan (TA). The sampling locations for the outgroup species are I, Slovakia (SL) for *M. spicilegus* and R, Spain (SP) for *M. spretus*. (B) shows the fraction of shared isoforms for pair-wise individual comparison. The fraction of shared isoforms between each pair of individuals is defined as the number of overlapping isoforms divided by the average number of detected isoforms of the two individuals to compare. Black boxes represent the interquartile range (IQR, distance between the first and third quartiles), with white dots in the middle to denote the median. The boundaries of the whiskers (also the ranges of violins) are based on the 1.5 IQR values for both sides. The statistical p-values of the fractions of shared isoforms between different comparison groups were computed using Wilcoxon rank sum tests. (C) shows the projection of the top two PCs of isoform variation in house mouse and outgroup individuals. Enlarged insets represent the results for the three populations from the subspecies of *M. m. domesticus*, as they cannot be well distinguished in the main figure. (D) and (E) show phylogenetic trees built based on isoform and SNP variants fixed within each population, respectively. Split nodes marked in yellow are the ones with bootstrap support value >70%.

The role of splicing noise

Since biochemical systems are never perfect, one should expect a certain number of errors in generating isoforms (Pickrell et al. 2010; Wan and Larson 2018). This could be considered as noise rather than being regulated through genetic polymorphisms or epigenetic effects.

Noise should be non-deterministic in the sense that the absolute number of isoforms generated by noise should increase with increased read sampling. This can be tested by a rarefaction analysis, where one takes increasingly larger random subsets of the reads in a given experiment and asks whether the number of isoforms keeps increasing. This is indeed the case. When using all reads for a given individual, one gets a linear increase in the number of isoforms with increased sampling without any signs of saturation (Figure 3A). However, when one does the same analysis for the high-confidence isoforms represented by at least 2 FLNC reads in a given individual, one gets an almost perfect saturation at the sequencing depth applied in our experiments (Figure 3B). The same patterns can be seen for individuals from each population sequenced (Supplemental Figures S8 and S9). Because of this difference in saturation behavior, we conclude that singletons are mostly the product of splicing errors, consistent with conclusions in previous studies (Pickrell et al. 2010; Saudemont et al. 2017).

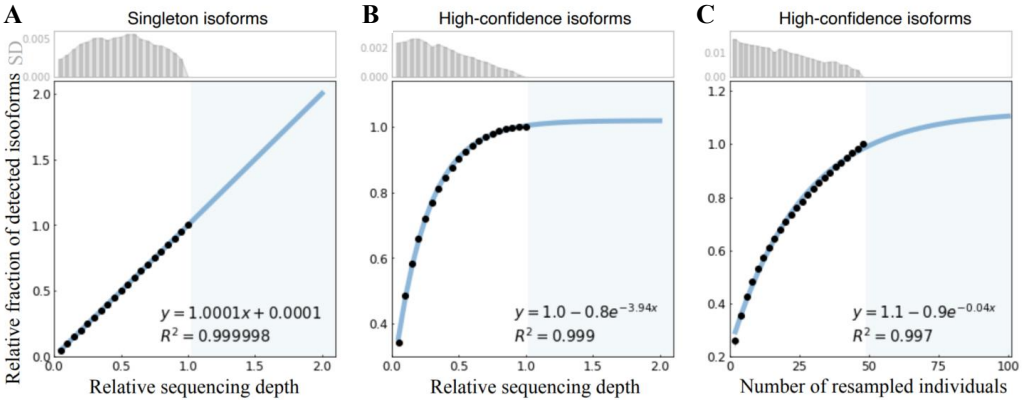

Figure 3 Saturation analysis on the sequencing depth and number of sampled individuals. (A) and (B) show the relative fractions of detected isoforms supported with singleton FLNC read versus two or more FLNC reads (high-confidence isoforms) with increasing random resampling of the Iso-Seq sequencing depth, respectively. The resampling sequencing depths were selected from 0.05 to 1, with a step size of 0.05. The blue area shows the prediction after doubling the actual Iso-Seq sequencing depth. The illustration is based on one randomly selected individual (GE3) in the GE population; the analogous results for individuals from other populations are provided in Supplementary Figures S8 and S9. (F) Relative fractions of detected isoforms with increasing random resampling sample sizes of individuals in the main experiment. The resampling sequencing sizes were selected from 2 to 48, with a step size of 2. The blue area shows the prediction after doubling the current sampling of mice individuals. The bar plots show the standard deviation (SD) of each resampling analysis.

Interestingly, random resampling analysis of subsamples across individuals shows that the number of detectable high-confidence isoforms remains unsaturated with the number of sampled individuals in our dataset (Figure 3C). That shows that more new isoforms are expected to show up when more individuals are analyzed, suggesting that these additional isoforms are more likely generated by genetic polymorphisms

244 between the individuals than by noise. However, some saturation should eventually be expected even at this
245 level since there is a limit to the maximum number of isoforms that can be reliably maintained in natural
246 populations (Benitiere et al. 2024).

247 In a further analysis of the noise effect, we make use of a recent discovery on the role of transposable
248 elements (TE) influencing splicing. Ilik et al. (Ilik et al. 2024) found that cells have developed mechanisms
249 to maintain splicing integrity with respect to excluding cryptic splice sites generated by TEs. If this process
250 is leaky, isoforms generated by noise effects should also include more TEs in their exons. We find that this
251 is indeed the case. Comparison of the transposon element (TE) insertions in singleton isoforms versus high-
252 confidence isoforms shows that the latter harbor a significantly lower fraction of TE fragment insertions
253 (Fisher's exact test, p-value $< 2.2 \times 10^{-16}$, Supplementary Figure S10).

254 Based on these analyses, we concluded that by excluding the singleton reads from the further analyses, we
255 are indeed excluding most of the effects of noise. Evidently, it is still possible that reads that occur more
256 than once are generated through noise effects due to the chromatin context in which they are transcribed or
257 special structures of their RNAs. However, we consider the set of high-confidence isoforms to be at least
258 highly enriched in variants that are not simply generated by errors in the splicing machinery.
259

260 *Alternative isoforms as population differentiation markers*

261 Given the high and comparable numbers of isoforms in wild mice brain transcriptomes across populations
262 (Table 1), we asked whether the isoform diversity landscape can distinguish individuals, *i.e.*, whether they
263 could contribute to individual differences. If this is the case, they could also be used to trace the divergence
264 trajectories of the populations.

265 A pairwise individual comparison of the sharing of isoforms reveals an increasingly larger fraction of shared
266 isoforms for individuals from different subspecies, different subspecies but same species, different
267 populations but same subspecies, and same populations (Figure 2B). The fraction degrees of shared isoforms
268 between different comparison groups are all statistically significant (p-value < 0.05). The overall principal
269 component analysis (PCA) shows clear clusters of individuals according to their origin. Still, considerable
270 diversity within each cluster implies that isoform diversity indeed confers a form of individuality to each
271 animal (Figure 2C). We further used the presence/absence matrix of fixed isoforms within each population
272 to build an overall phylogeny (Figure 2D), which has the same general topology as a phylogeny based on
273 the SNP variants called from Illumina RNA-Seq datasets from the same set of mice individuals (Figure 2E).

274 The above patterns were unlikely caused by the imbalance of sequencing depth for different mice individuals,
275 as the numbers of detected isoforms have reached saturation at the individual level (Figure 3B). These
276 findings remain valid when analyzing the isoforms observed in at least two individuals (Supplemental
277 Figure S11), further eliminating the possible dominating effects of low-abundance isoforms.

278 Given these observations, we performed an isoform frequency-based approach to detect the isoforms as
279 population-differentiating markers (see Methods). Each isoform was assigned a population differentiation
280 index (PDI) to indicate its power to differentiate populations. After applying a false discovery rate (FDR)
281 threshold of 0.05, we detected in total 113,008 isoforms (96% of all isoforms) that could differentiate
282 populations from house mouse and outgroup species (with significantly larger PDI values compared with

null distribution from 1,000 times random shuffling; see Supplemental Data S2). We conclude that isoforms can serve as effective markers to differentiate house mouse natural populations.

A high number of novel isoforms are absent in the reference annotation

To further characterize the features of the 117,728 high-confidence distinct isoforms, we compared them with those annotated in the GRCm39/mm39 reference genome from Ensembl v103 (Howe et al. 2021), built largely based on a single C57BL/6 lab mouse inbred strain, which has predominantly a genomic *M. m. domesticus* population background. Based on their alignment status to the Ensembl mouse transcriptome v103 (Howe et al. 2021), these isoforms were classified into eight distinct structural categories using SQANTI3 (Tardaguila et al. 2018) (Figure 4A): i) full splice match (FSM); ii) incomplete splice match (ISM); iii) novel in category (NIC); iv) novel not in category (NNC); v) Fusion (F); vi) genic (G); vii) antisense (A); viii) intergenic(I). The statistics on the number of isoforms from each structural category at the population level can be found in Table 1.

In total, we found only 51% of the 117,728 distinct isoforms matching perfectly to a whole (FSM, 34.9%) or subsection (ISM, 16.1%) of a reference annotated isoform, designated as known isoforms following the convention in (Leung et al. 2021; Naftaly et al. 2021). The remaining 49% (57,730) of the identified isoforms were missing in the Ensembl transcriptome (Figure 4B), including the ones deriving from the rearrangement and modification of annotated exons (novel combination of known splice sites or NIC: 23.8%; novel splice sites or NNC: 22.5%; and merging of adjacent transcripts or Fusion: 1.0%), from intronic regions (Genic: 0.2%), and from entirely novel gene loci (Antisense: 0.5%; Intergenic: 0.9%). Of note, the novel isoforms exhibit comparable high quality and reliability as the known isoforms, based on the confirmation of the transcription start site, splice junction, and transcript end site (Supplemental Figure S5C-E).

One may argue that the isoforms specific to outgroup species could contribute substantially to the novel isoform category, as the GRCm39/mm39 reference genome was built primarily based on a single C57BL/6 lab inbred strain (*i.e.*, *Mus musculus*). The individuals from the outgroup species indeed have an average of 27.1% of isoforms that are not registered in the mm39 reference annotation, slightly larger than the value of 25.2% in mice individuals belonging to *Mus musculus* (p-value = 0.003, Wilcoxon rank sum test, Supplemental Data S4). However, we still found that around 43% of the identified unique isoforms were missing in the reference annotation after excluding those isoforms detected only in individuals of outgroup species (Supplemental Figure S12B). Of note, the fraction of FLNC reads to support novel isoforms is generally lower than the fraction of novel isoforms for each mouse individual (Average value: 6.0% vs 25.5%, Supplemental Data S4).

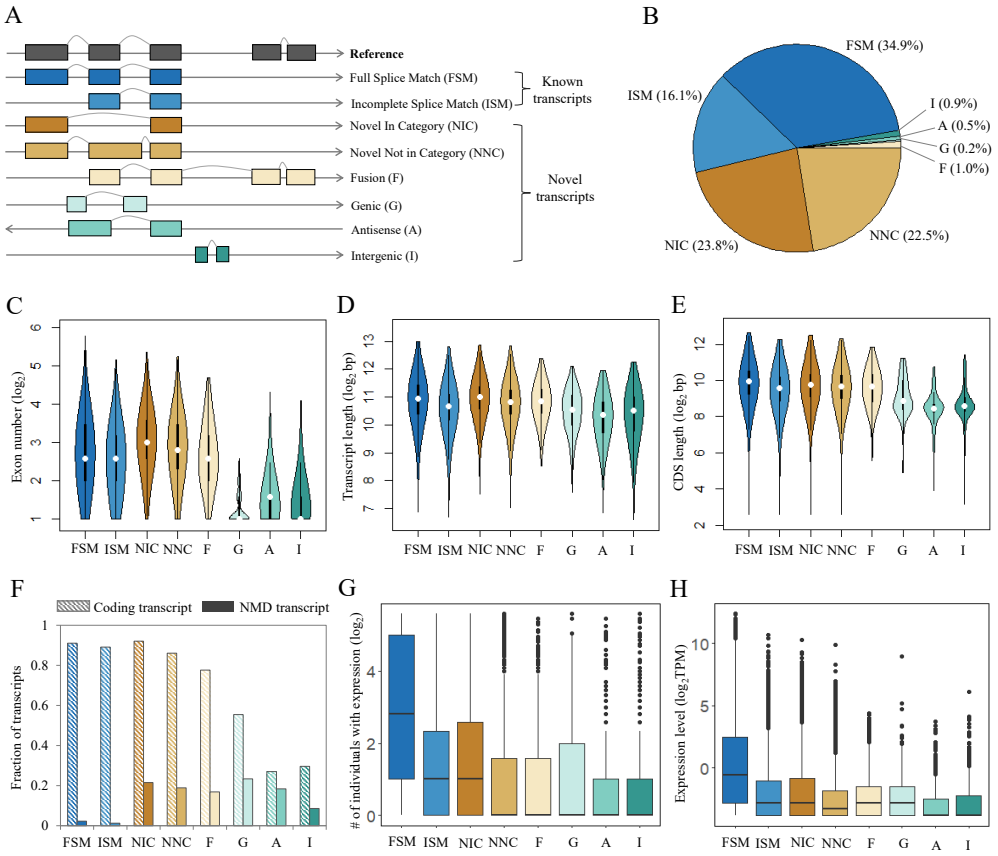

Figure 4 Characterization of all detected high-confidence isoforms. (A) Types and illustrations of identified isoforms. (B) Fraction distribution of isoform structural categories (see isoform annotations in Supplemental Data S2). (C)-(H) show the distributions of isoform types for distinct features. Isoforms with expression were defined as those with non-zero TPM values, and the expression levels were computed based on the number of supported FLNC reads using SQANTI3 (Tardaguila et al. 2018). Boxes represent the interquartile range (IQR, distance between the first and third quartiles), with white dots (or black lines) in the middle to denote the median. The boundaries of the whiskers (also the ranges of violins for panels C-E) are based on the 1.5 IQR values for both sides; black dots in G and H represent outliers.

Given that the current reference annotation is based on an isogenic strain, it represents nominally only the isoforms of a single individual but not the isoforms typical for a population or across populations. At the same time, it includes isoforms that are restricted to its population of origin. We have therefore compiled a set of 39,537 isoforms that are conserved in the house mouse and the outgroup species (marked in yellow in Supplemental Data S2). A substantial fraction (30.6%) of these isoforms is not included in the reference annotation (Supplemental Figure S12C). We propose that this conserved set of isoforms should be the best reference when comparing between mice and other species, *e.g.*, humans.

In comparison to known isoforms (FSM, ISM), novel isoforms deriving from annotated exonic regions (NIC, NNC, and F - which constitute the bulk of the new isoforms) show comparable exon numbers (Figure 4C), transcript length (Figure 4D) and CDS length (Figure 4E). The novel isoforms from intronic (G) and

337 unannotated gene loci (A, I) show generally lower values for all these features (Supplemental Table S2).
338 Notably, all the novel isoforms with coding potential have a significantly higher probability of becoming
339 degraded via the nonsense-mediated decay (NMD) process (Chang et al. 2007) due to premature translation-
340 termination codons (PTCs - detected by SQANTI3) than known isoforms (Figure 4F, mean 0.18 vs. 0.02,
341 Fisher's exact test, p-value < 2.2×10^{-16}). Most novel isoforms were found to be more restrictively expressed
342 in a smaller number of individuals, except for NIC, which are comparable to ISM in this respect (Figure
343 4G). The general expression levels of the novel isoforms, except A and I, are at a similar level as the known
344 ISM isoforms (Figure 4H). Regarding absolute isoform abundance, the newly discovered isoforms
345 contribute about 6% to the total number of expressed isoforms in the overall dataset, in contrast to 49% of
346 identified unique isoforms as novel ones (Figure 4B).

347

348 *Housekeeping genes are the major contributor to isoform diversity*

349 To analyze the characteristics of the gene loci that contribute significantly to the overall isoform diversity,
350 we classified all the detected gene loci into three roughly similar-sized classes based on their splicing
351 isoform numbers (Figure 5A): i) Few-isoform Genes (FG, with no more than two isoforms, n = 5,372), ii)
352 Many-isoform Genes (MG, with isoform number between three and eight, n = 5,012), and iii) Plenty-
353 isoform Genes (PG, with no less than nine isoforms, n = 4,628). Among all the 117,728 high-confidence
354 isoforms detected in the wild mice brain transcriptome, 4.3% are derived from the FG group, 18.2% from
355 the MG group, and the largest fraction (77.4%) from the PG group.

356 Based on the gene expression analysis of matched Illumina RNA-Seq dataset, we found that genes with
357 more splicing isoforms have a significantly higher expression level in the brain (Figure 5B, MG vs. FG: p-
358 value = 8.7×10^{-294}, PG vs. MG: p-value = 3.2×10^{-182}, two-sided Wilcoxon rank sum tests)**.** Additionally,
359 through analyzing the transcriptomic sequencing dataset from thirteen tissues of the *M. m. domesticus*
360 derived C57BL/6 inbred line (Lin et al. 2014) (Supplemental Data S1D), we observed a clear trend that
361 genes with more splicing isoforms tend to be expressed significantly more broadly, *i.e.*, with expression in
362 more tissues (Figure 5C, MG vs. FG: p-value = 8.2×10^{-129}, PG vs. MG: p-value = 4.2×10^{-17}, two-sided
363 Wilcoxon rank sum tests). Furthermore, gene ontology (GO) enrichment analysis on the PG group showed
364 that they are involved in a variety of biological processes for the maintenance of cellular function
365 (Supplemental Data S5), a common feature of housekeeping genes (Eisenberg and Levanon 2003). These
366 findings suggest that housekeeping genes contribute most to the overall isoform diversity.

367 Previous studies have shown that evolutionarily old genes usually have a broader tissue expression and
368 higher expression levels (Zhang et al. 2015). Thus, it can be hypothesized that genes with more splicing
369 isoforms tend to be evolutionarily older. We set out to test this hypothesis via a comparative analysis of the
370 gene age distribution pattern among the gene groups with different numbers of splicing isoforms, for which
371 the mouse gene age assignment data was retrieved from (Neme and Tautz 2013). Our analysis indeed
372 showed that there is a significant enrichment in evolutionarily older gene groups for those genes with more
373 splicing isoforms (Figure 5D, MG vs. FG: p-value = 4.1×10^{-15}, PG vs. MG: p-value = 1.5×10^{-7}, two-sided
374 Wilcoxon rank sum tests).

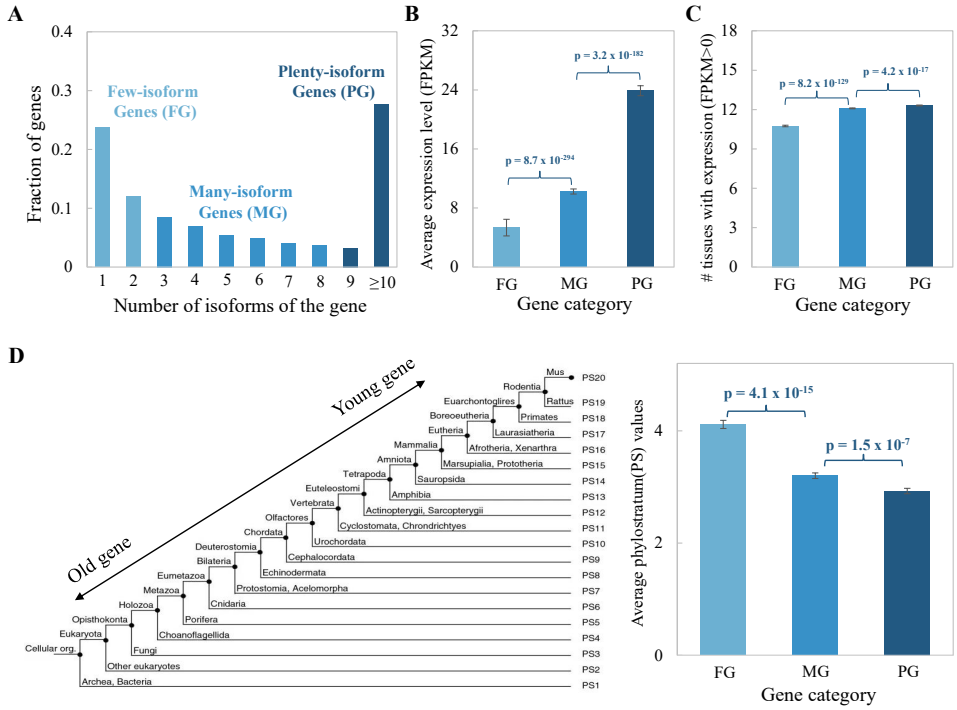

Figure 5 Characteristics of gene loci with different numbers of isoforms. (A) Gene categories were based on the number of isoforms of each gene. Three gene categories were classified with roughly the same number of genes in each group. (B) Comparison of the average gene expression level among the three gene categories. The average gene expression level was calculated based on the Illumina RNA-Seq generated in this study. (C) Comparison of the number of tissues with expression among the three gene categories. The transcriptomic sequencing data from 13 tissues of the *Mus musculus* C57BL/6 inbred line was retrieved from (Lin et al. 2014). The detectable gene expression in each tissue was defined as FPKM > 0. (D) Comparison of the average phylostratum (PS) values among the three gene categories. The PS assignment data for mouse protein-coding genes were retrieved from (Neme and Tautz 2013). The smaller PS values indicate the older gene groups. Error bars show standard errors of the mean (SEM) values of average gene expression levels, number of tissues with expression, and average PS values, respectively. Statistical p-values were computed using two-sided Wilcoxon rank sum tests.

Isoform expression in highly versus lowly expressed genes

It has previously been noted that the fraction of isoforms expressed as alternative isoforms from highly expressed genes is lower than that for lowly expressed genes (Sharon et al. 2013; Benitiere et al. 2024). We have analyzed this in our data by generating normalized FLNC read counts (TPM) as a proxy for the expression level of the respective isoforms from each gene. We then compared the top expressed (T) isoform for a given gene with the read counts of the remaining isoforms (R) from the same gene. We restrict this analysis to *M. musculus* populations, *i.e.*, excluding the outgroups, since many top expressed isoforms change in these outgroups. The average ratio R/T across all genes with at least two isoforms in at least one individual of the *M. musculus* populations (N = 9,111) is 1.03 (SD: 1.04). The same calculation for the top 10% expressed genes is 0.43 (SD: 0.63) and for the lowest 10% expressed genes is 1.11 (SD: 0.62) (Supplemental Data S6), *i.e.*, the overall fraction of alternative isoform molecules is about 3-fold lower for highly expressed genes compared to the lowest expressed genes (p-value = 2.02×10^{-147}, Wilcoxon rank sum test). Hence, while highly expressed genes have, on average, more alternative isoforms than lowly

expressed genes (see above), their relative expression level is much lower than for the alternative isoforms of lowly expressed genes. This could suggest constraints on highly expressed genes for generating too many new isoforms (Saudemont et al. 2017; Benitiere et al. 2024).

Local alternative splicing events contribute to isoform diversity

The full-length isoforms appear as a combination of different types of local alternative splicing (AS) events. Thus, it is useful to disentangle the relative contribution of each type of AS event to the overall isoform diversity. For this purpose, we used the SUPPA2 program (Trincado et al. 2018) to identify different types of splicing events in the complete set of high-confidence isoforms, including skipped exon (SE), retained intron (RI), alternative 5' splice site (A5), alternative 3' splice site (A3), mutually exclusive exon (MX), alternative first exon (AFE), and alternative last exon (ALE) (Figure 6A).

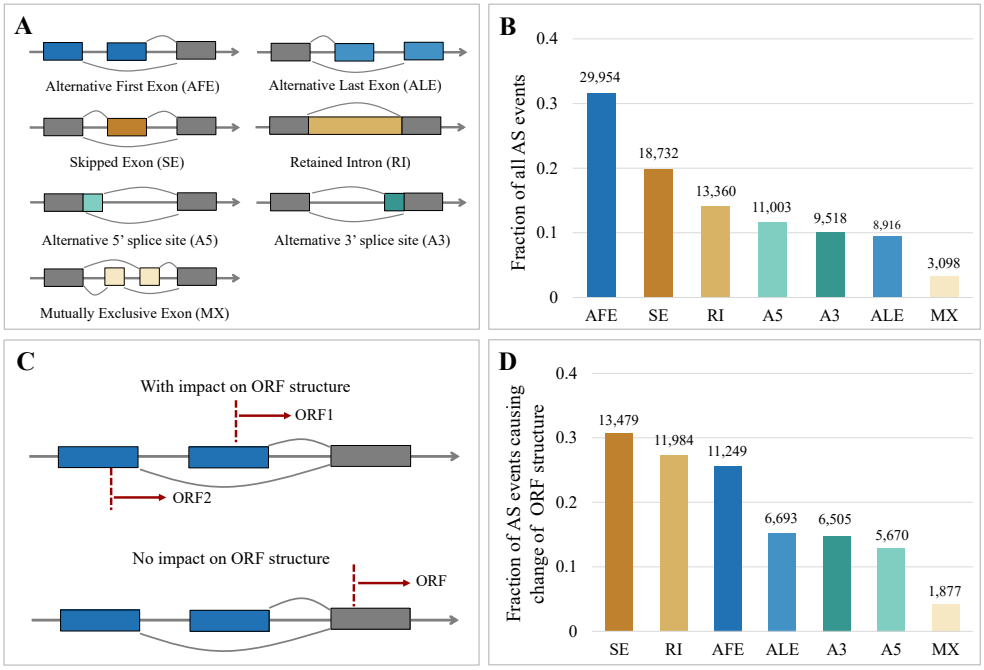

Figure 6 Distribution of different types of local AS events. (A) Types and illustrations of AS local events. (B) The distribution of all types of local AS events. (C) An example of AFE events that change ORF structures and similar situations for other types of local AS events. The dashed red lines indicate the in-frame start codon positions. (D) The distribution of all types of local AS events that impact respective ORF structures. The value above each bar in (B) and (D) indicates the number of respective types of local AS events.

Among all the 94,581 splicing events detected in all the isoforms (Figure 6B), AFE events contribute most to the overall isoform diversity (31.7%), followed by SE events (19.8%), RI events (14.1%), A5 (11.6%), A3 (10.1%), ALE (9.4%), and with MX as a minor contributor (3.3%). This finding is in line with the previous report on the AFE as the most prevalent splicing event for the overall transcriptome in the inbred

423 laboratory mouse cerebral cortex (Leung et al. 2021), suggesting a dominant role of using AFE to generate
424 alternative isoforms in mice brain transcriptomes.

425 AFEs would not necessarily impact the coding sequences (Landry et al. 2003). To address this issue, we
426 performed an additional analysis by collapsing the isoforms with the same coding sequence (*i.e.*, only
427 isoforms with predicted ORFs were considered) into a single unique ORF. We indeed observed a much
428 lower number (less than two-thirds) of unique ORFs than isoforms in each mouse individual (Supplemental
429 Figure S13). Based on the landing position of the start codon in relation to local AS events (Figure 6C), we
430 further enumerated the number of local AS events causing the change of the respective coding sequences.
431 We found that only 46.5% (43,978) of all the local splicing events impact the ORF structures (Figure 6D).
432 Compared to AFE, SE, and RI events are more prevalent among all the local AS types to contribute to ORF
433 diversity. The majority of AFE events (55%) would cause no change in the coding sequences while acting
434 as a major source to generate isoform diversity at the RNA level (Huang et al. 2021). These data illustrate
435 the distinct roles of local AS events in contributing to isoform and ORF diversity in wild mice brain
436 transcriptomes.

437

438 **Discussion**

439 We used PacBio Iso-Seq and Illumina RNA-Seq to characterize the full-length isoform diversity of the brain
440 transcriptomes in house mouse natural populations, resulting in the first and most comprehensive full-length
441 isoform category representation at a comparative population level to date. Via implementation of a separate
442 5' CAP selection step (Cartolano et al. 2016; Kuo et al. 2017), our optimized approach improved the
443 performance to enrich genuine full-length transcripts.

444 Our overall results confirm the conclusions from previous studies that the diversity of alternatively spliced
445 isoforms surpasses the current annotation level, even of exceptionally well-curated genomes, such as the
446 one from the mouse (Leung et al. 2021). Our study finds double as many isoforms as are currently annotated,
447 suggesting the widespread diversity of alternative isoforms in natural populations. Intriguingly, these
448 isoforms could be efficient markers to infer population relationships and resolve the phylogenetic tree of
449 house mouse natural populations and outgroups. This suggests that the isoform diversity reflects directly
450 the genetic polymorphisms segregating in these populations. Note that the mice used for this study were
451 reared under tightly controlled laboratory conditions to eliminate possible environmental influences on
452 isoform diversity.

453 Interestingly, evolutionarily old housekeeping genes with overall high expression in many tissues show the
454 largest number of new splice variants on average, likely due to the longer gene length and a larger number
455 of exons for the evolutionarily old housekeeping genes (Zhang et al. 2015). Indeed, we found plenty-isoform
456 genes are significantly longer (indicated by the longest transcript length) and have significantly more exons
457 (Supplemental Figure S14), potentially allowing more space for alternative splicing machinery to act on.

458 The focus on full-length transcripts revealed that new 5'-exons are the relatively most abundant source of
459 new isoforms, followed by the "skipped exon" and "retained intron" variants, which were previously thought
460 to be the most prevalent ones (Grau-Bove et al. 2018). Many "alternative first exon" isoforms might
461 originate from new promotors that can easily develop upstream of existing genes. This is in line with the

462 realization that enhancers as regulatory elements can also assume promotor functions (Andersson and
463 Sandelin 2020). Only about half of the new splice variants affect the annotated ORF of the respective genes,
464 implying that the ORF diversity generated through alternative splicing is lower than the one at the isoform
465 level. However, new short ORFs or alternative ORFs that may arise in the alternatively spliced isoforms are
466 yet to be studied (Leong et al., 2022).

467 Our dataset allows to define isoforms that should be of particular interest for functional comparisons across
468 larger evolutionary distances, including humans. The currently annotated mouse genome also includes the
469 isoforms that are population-specific for the subspecies from which the C57Bl/6 was derived. Most of these
470 will have specifically arisen in this lineage and are, therefore, of less interest for broader functional
471 comparisons. With our comparative data, however, we can define the set of isoforms that are typically found
472 across multiple mouse species, including new ones that were so far missing from the annotation. We have
473 compiled this more informative and more inclusive set of isoforms (Supplemental Data S7), which will be
474 of particular use for broader comparative studies between mice and other species.

475

476

477

478 **Methods**

479 *Ethics statement*

480 All the mice were kept according to FELASA (Federation of European Laboratory Animal Science
481 Association) guidelines, with the permit from the Veterinäramt Kreis Plön: 1401-144/PLÖ-004697. The
482 samples used for this study were derived as organ retrieval under permit number 1158 (following §4 German
483 TSchVersV) from the respective animal welfare officers at the University of Kiel (Prof. Schultheiss and
484 Mrs. Vieten).

485

486 *Sample collection and RNA extraction*

487 49 male mice individuals were sampled in this study, including one being used in the Iso-Seq library
488 preparation protocol optimization experiment (Supplemental Data S1A and S1B). Eight individuals were
489 chosen for each of the following populations covering all three major subspecies of the house mouse (*Mus*
490 *musculus*): Germany, France, and Iran populations from *Mus musculus domesticus*, Kazakhstan population
491 from *Mus musculus musculus*, and Taiwan population from *Mus musculus castaneus*. We also included four
492 individuals from each of the two outgroup species, *Mus spretus* and *Mus spicilegus*. All mice were derived
493 from previously wild-caught founder mice and were maintained in an outbred scheme under standard rearing
494 techniques, which ensure a homogeneous environment (Harr et al. 2016). Each mouse individual was
495 obtained from one distinct, unrelated breeding family. Thus, the relatedness between individuals, especially
496 from the same population, should be minimized (see Supplemental Data S1E for pairwise relatedness
497 estimates).

498 Mice were sacrificed at approximately ten weeks of age by CO_2 asphyxiation followed immediately by
499 cervical dislocation. The whole brain was dissected and immediately frozen in liquid nitrogen within 5
500 minutes post-mortem. Total RNAs were extracted and purified using RNeasy lipid tissue kits (Qiagen, The
501 Netherlands). RNA was quantified using Qubit Fluorometers (Invitrogen, Thermo Scientific, USA), and
502 RNA quality was assessed with 2100 Bioanalyzer (RNA Nanochip, Agilent Technologies, USA). All
503 samples with RIN values above 8.5 were then used for both PacBio and Illumina transcriptome sequencing
504 at the Max Planck-Genome-Centre Cologne.

505

506 *Selection of cDNA library enrichment protocol for PacBio Iso-Seq*

507 It has been reported that the TeloPrime full-length cDNA Amplification kit, which selectively synthesizes
508 cDNA molecules from mRNAs carrying a 5' CAP in comparison to the standard PacBio cDNA library
509 preparation protocol, provides a better solution to enrich for actual full-length transcripts (Cartolano et al.
510 2016). In this study, we selected one male mouse from the Taiwan population (Supplemental Data S1A) to
511 test the performance of TeloPrime-based protocols in the real world.

512 We applied three distinct cDNA library enrichment protocols for the RNA sample extracted from the same
513 mice individual: i) standard PacBio Clontech SMARTer PCR cDNA Synthesis kit (Clontech Laboratories,
514 Inc.); ii) TeloPrime Full-Length cDNA Amplification Kit v1 (Lexogen GmbH), with the combination of the
515 SMARTer PCR cDNA Synthesis kit; iii) TeloPrime Full-Length cDNA Amplification Kit v2 (Lexogen
516 GmbH), with the combination of the SMARTer PCR cDNA Synthesis kit. The former protocol selectively
517 synthesizes cDNA molecules from transcripts with a poly(A) tail and uses cDNA primers (5'
518 AAGCAGTGGTATCAACGCAGAGTACATGGGG; 3' GTACTCTGCGTTGATACCACTGCTT). In
519 contrast, the latter two protocols synthesize cDNA molecules from transcripts with both a 5' CAP and a
520 poly(A) tail, and uses cDNA primers (5' TGGATTGATATGTAATACGACTCACTATAG; 3'
521 GTACTCTGCGTTGATACCACTGCTT). The two cDNA primer sets differ only in the 5'end, while the
522 segments for the 3'end are the same. TeloPrime-based kit V2 includes updated reaction conditions in
523 comparison with kit V1, while the method of cDNA generation remains unchanged. For each protocol, we
524 used 1 ug homogeneous RNA as input to generate the cDNA library. The cDNAs were not size-selected,
525 and PacBio libraries were prepared with the SMRTbell Template Prep Kit 1.0 (Pacific Biosciences) and
526 sequenced on the PacBio Sequel I with Sequel DNA polymerase and binding kit 3.0 and sequencing
527 chemistry version 3.0 for 1200 min. Each cDNA library was sequenced on one SMRT cell of the same
528 sequencing run.

529 We analyzed the sub-reads for each SMRT cell separately following the IsoSeq3 pipeline (v3.4.0;
530 https://github.com/PacificBiosciences/IsoSeq) and aligned the resulting isoforms to the mouse genome
531 (GRCm39/mm39) using minimap2 (v2.24-r1122) (Li 2018), with the computational protocol indicated in
532 the below text. The alignment results from the above three cDNA libraries were compared to the coordinates
533 of transcripts annotated in Ensembl (v103) using gffcompare (v0.12.2) (Pertea and Pertea 2020).

534 Based on the detected isoforms in the Clontech library, we compare the transcripts with 5' end truncation
535 (*i.e.*, lacking at least the first exon, N=3,567) and the intact transcripts compared to reference annotation
536 (N=4,199) at two different levels: i) the terminal exon length at 5'end; ii) the RNA structure property. The

537 RNA structure property was measured as the minimum free energy (MFE) of the best predicted structure
538 using RNAfold v2.6.4 with the following parameters "-p -d2 –noLP" (Gruber et al. 2008).

539

540 *PacBio Iso-Seq and Illumina RNA-Seq sequencing*

541 The initial experimental tests showed that our newly developed TeloPrime-based cDNA library preparation
542 protocol could provide a better solution to enrich for actual full-length transcripts, compared to the standard
543 PacBio cDNA library preparation protocol. Hence, the TeloPrime Full-Length cDNA Amplification Kit v2
544 (Lexogen GmbH) was utilized to construct PacBio IsoSeq cDNA libraries. One µg total RNA from each
545 individual was used as input, and double-strand cDNA was produced by following the manufacturer's
546 instructions, except that an alternative oligo-dT primer from the SMARTer PCR cDNA Synthesis kit
547 (Clontech Laboratories, Inc.), which also included a random 10mer sequence as a unique molecule identifier
548 (UMI) after each sequence. The cDNAs were not size-selected, and PacBio libraries were prepared with the
549 SMRTbell Template Prep Kit 1.0 (Pacific Biosciences) and sequenced on the PacBio Sequel I with Sequel
550 DNA polymerase and binding kit 3.0 and sequencing chemistry version 3.0 for 1200 min. Each library was
551 sequenced on three SMRT cells to achieve sufficient coverage.

552 Poly(A) RNA from each sample was enriched from 1 µg total RNA by the NEBNext® Poly(A) mRNA
553 Magnetic Isolation Module (Catalog #: E7490, New England Biolabs Inc.). RNA-Seq libraries were
554 prepared using NEBNext Ultra™ II Directional RNA Library Prep Kit for Illumina (Catalog #: E7760, New
555 England Biolabs Inc.), according to manufacturer's instructions. A total of eleven PCR cycles were applied
556 to enrich library concentration. Sequencing-by-synthesis was done at the HiSeq3000 system in paired-end
557 mode 2 x 150bp. Raw sequencing outputs were converted to fastq files with bcl2fastq (v2.17.1.14).

558

559 *RNA-Seq read QC and data processing*

560 We trimmed and filtered the low-quality raw fastq reads for each sample separately using the fastp program
561 (v0.20.0; --cut_front --average_qual 20 --length_required 50) (Chen et al. 2018) and only included the
562 paired-end reads with a minimum length of 50bp and average quality score of 20 for further analysis.

563 The filtered fastq reads were aligned to mouse GRCm39/mm39 reference genome sequence with STAR
564 aligner v2.7.0e (Dobin et al. 2013), taking the mouse gene annotation in Ensembl v103 (Howe et al. 2021)
565 into account at the stage of building the genome index (--runMode genomeGenerate --sjdbOverhang 149).
566 The STAR mapping procedure was performed in two-pass mode, and some of the filtering parameters were
567 tweaked (personal communication with STAR developer: see
568 https://github.com/alexdobin/STAR/issues/1147; --runMode alignReads –twopassMode Basic --
569 outFilterMismatchNmax 30 --scoreDelOpen -1 --scoreDelBase -1 --scoreInsOpen -1 --scoreInsBase -1 --
570 seedSearchStartLmax 25 --winAnchorMultimapNmax 100), in order to compensate the sequence
571 divergences of individuals from various populations and species (Zhang et al. 2021). With this optimized
572 mapping pipeline, a similar alignment rate was reached for all the samples (Supplemental Data S1C). The
573 alignment bam files were taken for further analysis.

574

575 *SNP variants calling and individual relatedness analysis*

576 We followed the general GATK version 4 Best Practices to call genetic variants from Illumina RNA-seq
577 data. We first sorted the above alignment bam data using samtools v1.9 (Li et al. 2009), and marked
578 duplicates using PICARD v2.8.0 (http://broadinstitute.github.io/picard). Reads with N in the cigar were split
579 into multiple supplementary alignments and hard clips mismatching overhangs using the SplitNCigarReads
580 function in GATK v4.1.9. By using BaseRecalibrator and ApplyBQSR functions in GATK, we further
581 recalibrated base quality scores with SNP variants that were called with the genomic sequencing dataset of
582 the mice individuals from the same populations (Zhang et al. 2021) to get analysis-ready reads. Following,
583 we called raw genetic variants for each individual using the HaplotypeCaller function in GATK and jointly
584 genotyped genetic variants for all the individuals using the GenotypeGVCFs function. We only retained
585 genetic variants that passed the hard filter "QD < 2.0 || FS > 60.0 || MQ < 40.0 || MQRankSum < -12.5 ||
586 ReadPosRankSum < -8.0 || SOR > 3.0" for further analysis (Zhang et al. 2021).

587 We used the relatedness2 option of VCFtools v0.1.14 (Danecek et al. 2011) to assess pairwise individual
588 relatedness for all possible pairs of mice individuals, based on only bi-allelic SNP variants with no more
589 than 20% missing data and locating within complete linear chromosomes, thinned to 1 SNP every 1 Mb
590 (Harr et al. 2016). We defined that relatedness category based on the expected ranges of kinship coefficients
591 ('Phi'), according to the primary reference of the KING method (Manichaikul et al. 2010). The detailed
592 relatedness information of all possible individual pairs can be found in Supplemental Data S1E.

593

594 *Iso-Seq read QC and data processing*

595 We analyzed the raw sub-reads for each SMRT cell separately following the IsoSeq3 pipeline (v3.4.0).
596 Circular consensus sequences (CCS) were generated from sub-reads using the CCS module in polish mode
597 (v6.0.0; --minPasses 3 --minLength 50 --maxLength 1000000 --minPredictedAccuracy 0.99) of the IsoSeq3
598 pipeline, and the CCS reads generated in three SMRT cells for the same sample were merged. We trimmed
599 the corresponding cDNA primers as shown above and orientated the CCS reads using the lima program with
600 the specialized IsoSeq mode (v2.0.0; --isoseq). The 10mer UMI following each CCS read was tagged and
601 removed using the tag module of the IsoSeq3 pipeline (--design T-10U). Following this, we identified the
602 processed CCS reads as full-length and non-chimeric (FLNC), based on the presence of a ploy(A) tail and
603 absence of concatemer using the refine module of the IsoSeq3 pipeline (--require-polya). We further
604 performed PCR deduplication based on the UMI tag information using the dedup module of the IsoSeq3
605 pipeline (default parameters). After this deduplication step, only one consensus FLNC sequence per founder
606 molecule in the sample was kept. We then performed *de novo* clustering of the above reads using the cluster
607 module of the IsoSeq3 pipeline and kept only the high-confidence isoforms supported by at least 2 FLNC
608 reads for further analysis.

609 We aligned these isoforms of each sample to the GRCm39/mm39 reference genome sequence using the
610 minimap2 (v2.24-r1122; -ax splice:hq -uf --secondary=no -C5 -O6,24 -B4) (Li 2018), with parameter setting
611 following the best practice of Cupcake pipeline (Gordon et al. 2015). The alignment bam files were further
612 sorted using the samtools program (v1.9) (Li et al. 2009). We collapsed redundant isoform models for each
613 sample based on the above sorted alignment coordinate information using the collapse module of the TAMA
614 program (-d merge_dup -x capped -m 5 -a 1000 -z 30 -sj sj_priority) (Kuo et al. 2020). The rationales for

615 defining redundant isoform models are shown in the Supplemental Text of Methods. Finally, isoforms
616 across all 48 samples were merged into a single non-redundant transcriptome using the merge module of
617 the TAMA program (-d merge_dup -m 5 -a 1000 -z 30) (Kuo et al. 2020), with the same parameter setting
618 as the above collapse step.

619

620 *Iso-Seq transcriptome classification and filtering*

621 We performed the quality control analysis for the above merged non-redundant PacBio Iso-Seq
622 transcriptome using SQANTI3 v4.2 (Tardaguila et al. 2018), with the input datasets of Ensembl v103 (Howe
623 et al. 2021) GRCm39/mm39 reference genome and gene annotation, FLNC read counts, Isoform expression
624 levels and STAR output alignment bam files and splice junction files from RNA-Seq short reads, mouse
625 transcription start sites (TSS) collected in refTSS database v3.1 (Abugessaisa et al. 2019), and curated set
626 of poly(A) sites and poly(A) motifs in PolyASite portal v2.0 (Herrmann et al. 2020).

627 We filtered out isoforms of potential artifacts mainly by following (Tardaguila et al. 2018). Mono-exonic
628 transcripts were excluded, as they tend more likely to be experimental or technical artifacts (Tardaguila et
629 al. 2018). Isoforms with unreliable 3'end because of a possible intrapriming event (intrapriming rate above
630 0.6) were also removed from the dataset. We kept the remaining isoforms that met both of the following
631 criteria: 1) no junction is not labeled as RT-Switching; 2) all junctions are either canonical (GT/AG; GC/AG;
632 AT/AC) or supported by at least three spanning reads based on STAR junction output file. All isoforms that
633 passed the above filters were taken for further analysis.

634 Given their matching status to the Ensembl mouse transcriptome v103 (Howe et al. 2021), the above
635 isoforms were classified into eight distinct categories using SQANTI3 (Tardaguila et al. 2018): i) Full Splice
636 Match (FSM, matching perfectly to a known isoform); ii) Incomplete Splice Match (ISM, matching to a
637 subsection of a known isoform); iii) Novel In Category (NIC, with known splice sites but novel splice
638 junctions); iv) Novel Not in Category (NNC, with at least one unannotated splice site); v) Fusion (F, fusion
639 of adjacent transcripts); vi) Genic (G, overlapping with intron); vii) Antisense (A, on the antisense strand of
640 an annotated gene); viii) Intergenic (I, within the intergenic region). The isoforms matching perfectly to a
641 whole (FSM) or subsection (ISM) of reference annotated transcripts are designated known isoforms, and
642 the others as novel isoforms.

643 We evaluated the reliability of isoforms from each category, based on the reference annotation and empirical
644 information, from three distinct aspects separately: i) transcription start site (TSS); ii) transcript end site
645 (TES); iii) splice junction (SJ). Compared to the well-support FSM isoforms, the isoforms from other
646 categories show reduced confidence levels in terms of TSS (Supplemental Figure S5B) but no reduction for
647 TES and SJ (Supplemental Figure S5D and 5E). This might hint at a failure to capture accurate TSS for
648 those transcripts (Tardaguila et al. 2018). For instance, it is still possible that some ISM isoforms came from
649 partial fragments due to the imperfect targeting of 5' CAP or the degradation of transcripts in the later steps.
650 To address this concern, we further excluded the non-FSM transcripts without support for TSSs
651 (Supplemental Figure S5C).

652

653 *Rarefaction and subsampling*

654 We investigated whether the PacBio Iso-Seq data provide sufficient coverage to detect all the isoform
655 diversity for the given sequencing depth of a single individual and the number of sampled individuals in the
656 experiment. Concerning the sequencing depth at the individual level, we randomly selected one sample from
657 each of the seven assayed populations and subsampled portions of FLNC reads from each sample chosen
658 for 100 times, ranging from 5% to 100%, at 5% intervals, and computed the fraction and variance of detected
659 isoforms for each round of subsampling. Regarding the number of sampled individuals, we subsampled
660 subsets of all the 48 assayed individuals for 100 times, ranging from 2 to 48, at an interval of 2, and computed
661 the fraction and variance of detected isoforms for each round of subsampling.

662 We tested two alternative models to determine whether the number of detected isoforms would continue to
663 increase or has approached saturation (Neme and Tautz 2016): a generalized linear model with logarithmic
664 behavior (ever-increasing) or a self-starting nonlinear regression model (saturating). The best fit was
665 decided based on the minimum BIC value between the two models, and the saturating model was the best
666 fit for both lines of analysis. All the analyses were performed in R v4.2.3, using the functions glm, nls,
667 SSasymp, and BI from the "stats" package (Team 2022).

668

669 *Test on the influence of noise on isoform diversity*

670 We analyzed the influence of noise on isoform diversity using two different tests. For the first test, we
671 extracted the list of isoforms supported by singleton FLNC reads in the de novo clustering step and filtered
672 out potential artifacts using the same procedure as shown above. We performed the rarefaction analysis to
673 test whether the number of singleton-supported isoforms has reached saturation with the sequencing depth
674 at the individual level, following the abovementioned pipeline. We further compared the saturation curves
675 between the isoforms represented by singleton FLNC reads and those represented by two or more FLNC
676 reads (*i.e.*, high-confidence isoforms).

677 For the second test, we annotated the inserted transposon element (TE) fragments in the singleton and high-
678 confidence isoforms using Repbase eukaryotes library v16.02 (Bao et al. 2015), which represents the largest
679 TEs database for eukaryotes. We used Repeatmasker v4.0.5 (Tempel 2012) to mask the isoforms against
680 the Repbase database with parameters "-nolow -no_is -norna -parallel 1". Only the TE fragments longer
681 than 10bp in length were included for further analysis. As several TE types might share the same coordinates,
682 we removed overlapping TEs to retain a single most appropriate TE based on a series of criteria: i) if a TE
683 insertion is entirely matching with another one with a different TEs type, the one with a larger mapping
684 score was retained; ii) If two TE fragments overlapped partially, the overlapped part was assigned to the
685 one with larger mapping score, then remaining part for the other TE, and was deleted if shorter than 10bp
686 in length. This filtering was repeated across all pairs of overlapping domains until the defined conditions
687 were satisfied. The TE insertion information for high-confidence and singleton isoforms can be found in
688 Supplementary Data S2 and S3.

689

690

691 *Association between transcript pattern and population divergence*

692 Based on three lines of analysis, we explored the association between individual isoform presence patterns
693 and population divergence. Firstly, we calculated and compared the fraction of shared isoforms between all
694 possible pairwise combinations from different species, from different subspecies but the same species (n =
695 448), from different populations but the same subspecies, and from the same populations. Secondly, we
696 performed PCA on the individual isoform landscape using the R package ggfortify v0.4.16 (https://cran.r-
697 project.org/web/packages/ggfortify/index.html). Additional PCAs were conducted for the subspecies *M. m.*
698 *domesticus*, given that more closely related populations were assayed in this study.

699 Lastly, we built a phylogenetic tree for the seven assayed populations using the R package "ape" v5.7-1
700 (Paradis and Schliep 2019), based on each population's presence/absence matrix of fixed isoforms.
701 Euclidean distance was used as the distance measure between each pair of populations, and the neighbor-
702 joining tree estimation function was used to build the phylogenetic relations. The boot.phylo function
703 implemented in the same R package was used to perform 1,000 bootstrap replications, and population split
704 nodes of high confidence were taken as the ones with at least 70% bootstrap support values. For comparison,
705 we constructed another phylogenetic tree with the SNP variants that were called from the Illumina RNA-
706 Seq dataset generated in this study (shown in the above text), for which the same set of mice individuals
707 was used. To reduce computation complexity, we performed LD pruning on the SNP data set by using
708 PLINK v1.90b4.6 (Purcell et al. 2007), removing one of a pair of SNPs with LD $\geqslant$0.2 in a sliding window
709 of 500 SNPs and stepwise of 100 SNPs. The same procedure was followed to build the phylogenetic tree,
710 as it was done for the analysis of isoforms.

711

712 *Detection of population differentiation isoform markers*

713 We calculated population differentiation index (PDI) values for each isoform using a similar approach to
714 analyze population differentiating retroCNVs (Zhang and Tautz 2022). A larger PDI value generally
715 indicates greater power to use the presence status of the respective isoform to distinguish populations. The
716 computation of the PDI value for each isoform follows:

717 $$\mathrm{PDI} = \frac{\mathrm{P}(1-\mathrm{P}) - \sum_{i=1}^{\mathrm{N}} \mathrm{R}_i * \mathrm{P}_i * (1-\mathrm{P}_i)}{\mathrm{P}(1-\mathrm{P})} \quad (1)$$

718 $$\mathrm{R}_i = \mathrm{N}_i \,/\, \sum_{i=1}^{\mathrm{N}} \mathrm{N}_i \quad (2)$$

719 In the first equation, N represents the number of assayed populations (*i.e.*, 7), P_i is the frequency of the focal
720 isoform in the *i*th population, and P is the overall frequency in all the assayed populations. The definition
721 of R_i is shown in the second equation and is computed as the number of individuals of the *i*th population
722 (N_i) divided by the total number of individuals from all populations. We tested the significance of the PDI
723 value for each isoform with a randomization test in which individual labels were randomly shuffled 1,000
724 times while population sizes remained the same. We calculated the p-value by comparing the observed PDI
725 for each isoform against the PDI values from the randomized null distribution. Isoforms with significant
726 PDI values after multiple testing corrections (FDR < 0.05) were considered population differentiation
727 isoform markers.

728

729 *Feature characterization of all the isoforms*

730 We characterized the features of all the detected isoforms from seven different aspects: i) exon number; ii)
731 isoform length; iii) CDS length; iv) fraction of coding isoforms; v) fraction of NMD isoforms; vi) the
732 number of individuals with expression; vii) isoform expression level. All these feature results were extracted
733 from the output of SQANTI3 analysis.

734 In the SQANTI3 pipeline (Tardaguila et al. 2018), the potential coding capacity and ORFs from the isoform
735 sequences were predicted using the GeneMarkS-T (GMST) algorithm (Tang et al. 2015). An NMD isoform
736 is designated if there's a predicted ORF, and the CDS ends at least 50bp before the last junction for the
737 respective isoform. The expression level of each isoform for each sample was computed based on the
738 number of supported FLNC reads and normalized in the unit of TPM (transcript per million). Isoforms with
739 expression in respective tissues were defined as the ones with non-zero TPM values. In addition, we
740 quantified the expression of each isoform using another program named Kallisto v0.46.2 (Bray et al. 2016),
741 for which the expression quantification was based on the alignment of Illumina RNA-Seq data to the merged
742 isoform dataset derived from PacBio Iso-Seq data, as shown in the above text.

743

744 *Feature characterization of gene loci with different number of isoforms*

745 We classified all the detected gene loci into three roughly similar-sized classes, based on their splicing
746 isoform numbers: i) Few-isoform Genes (FG, with no more than two isoforms, n = 5,372), ii) Many-isoform
747 Genes (MG, with isoform number between three and eight, n = 5,012), and iii) Plenty-isoform Genes (PG,
748 with no less than nine isoforms, n = 4,628). We characterized the features of the gene loci with different
749 numbers of isoforms from three aspects, *i.e.*, gene expression pattern, gene age distribution pattern, and
750 gene ontology (GO) functional term enrichment.

751 Firstly, we exploited two Illumina RNA-seq datasets for the gene expression pattern analysis: i) the one
752 generated in this study for the whole brain of 48 mice individuals; ii) a published dataset from thirteen
753 tissues (adipose tissue, adrenal gland, brain, heart, kidney, liver, lung, pancreas, sigmoid colon, small
754 intestine, spleen, ovary, and testis) of the *M .m. domesticus* C57BL/6 inbred line (Lin et al. 2014). The raw
755 fastq data for both datasets were trimmed, filtered, and aligned to the mouse GRCm39/mm39 reference
756 genome, as shown in the above text. We counted the fragments uniquely mapped to the annotated genes in
757 Ensembl v103 using featureCounts v1.6.3 (Liao et al. 2014) in reversely stranded mode, excluding multi-
758 mapping reads and those with alignment quality below 5 (-s 2 –Q 5). Gene expression levels were calculated
759 and transformed into a log2 scale of FPKM (Fragments Per Kilobase of transcript per Million mapped
760 fragments) based on the gene's isoform length and the number of mapped fragments in the data set from
761 each sample. For the first dataset, the average gene expression level was computed as the mean value in all
762 the assayed 48 samples. For the second dataset, the number of tissues with expression for each gene was
763 defined as the count of tissues with non-zero FPKM values. The statistical significances of the expression
764 patterns between pairwise groups of gene sets were computed using two-sided Wilcoxon rank sum tests.

765 Secondly, we analyzed and compared the evolutionary gene age pattern among three gene groups, taking
766 advantage of the mouse gene age assignment data from Neme *et al.* (Neme and Tautz 2013). In brief, each
767 mouse protein-coding gene was dated and given phylostratum (PS) assignment by inferring the absence and
768 presence of orthologs along the phylogenetic tree. The statistical significances of PS values between
769 pairwise groups of gene set were computed using two-sided Wilcoxon rank sum tests.

770 Lastly, we performed GO enrichment analysis on the genes from the PG group using GOSeq v1.50.0 (Young
771 et al. 2010), without correction of gene length differences. Only significant BP (biological process) terms
772 after multiple testing corrections (FDR < 0.05) were listed in this study.

773

774 *Calculation of isoform expression for highly versus lowly expressed genes*

775 We focused on the genes with at least two isoforms in at least one individual of the *M. musculus* populations,
776 resulting in a total of 9,111 gene loci for further analysis. The isoform data in outgroups were excluded for
777 this since many top-expressed isoforms can change in these outgroups. We used the normalized FLNC read
778 counts (TPM) as a proxy for the expression level of isoforms and the sum of expression of all isoforms
779 belonging to a given gene locus. The final isoform/gene expression values were averaged across all the *M.*
780 *musculus* individuals.

781 We calculated each gene's top expressed isoform read counts (T) by the read counts of the remaining
782 isoforms (R) from the same genes. These calculations were performed for all the genes, the top 10%
783 expressed genes and lowest 10% expressed genes, separately. The statistical significance on the ratio
784 difference between the top 10% expressed genes and lowest 10% expressed genes was computed using
785 Wilcoxon rank sum test.

786

787 *Analysis of local AS events*

788 We used the SUPPA2 program (Trincado et al. 2018) to identify local alternative splicing (AS) events in
789 the transcriptome. These local AS events are categorized into seven groups, including skipped exon (SE),
790 retained intron (RI), alternative 5' splice site (A5), alternative 3' splice site (A3), mutually exclusive exon
791 (MX), alternative first exon (AFE), and alternative last exon (ALE).

792 For the isoforms with predicted ORFs, we analyzed how the local AS events change the ORF structures. In
793 case the start codon position of the ORF lands in the region of a local AS event, the focal AS event is defined
794 to cause a change in the respective coding sequence. On the other hand, in case the start codon position of
795 the ORF falls downstream of the local AS event, it does not influence the ORF structure.

796

797 **Data access**

798 The raw PacBio Iso-Seq data and Illumina RNA-Seq data generated in this study have been submitted to
799 the European Nucleotide Archive (ENA; https://www.ebi.ac.uk/ena) under study accession number
800 PRJEB54001 (test experiment), PRJEB54000 and PRJEB53988 (the main experiment). Alignment bam

801 files, GTF track data, and SNP VCF files are stored at the ftp site:
802 https://wwwuser.gwdg.de/~evolbio/evolgen/wildmouse/mouse_population_isoform/ and supplemental
803 data at https://edmond.mpg.de/dataset.xhtml?persistentId=doi:10.17617/3.3RLIHR All the essential
804 computing codes are provided as Supplemental Data 8, and related data files are available at GitLab:
805 https://gitlab.gwdg.de/wenyu.zhang/mouse_population_isoform/.

806

807 **Competing interest statement**

808 The authors declare that they have no conflicts of interests.

809

810 **Acknowledgements**

811 We appreciate Christine Pfeifle, Heike Harre, Milan Jovicic, and Mustafa Al-Ameer for mice breeding and
812 handling. We thank Carsten Fortmann-Grote for computing assistance and Chen Xie for helpful discussion.
813 We thank Henrik Kaessmann for helpful suggestions on the manuscript. Computing was supported by the
814 high-performance computing clusters of the Max Planck Institute for Evolutionary Biology and School of
815 Ecology and Environment at Northwestern Polytechnical University. This work was supported by
816 institutional funding through the Max Planck Society to D.T. and W.Z., and the Fundamental Research
817 Funds for the Central Universities in China (grant number: G2022KY05106), National Natural Science
818 Foundation of China (grant number: 32370665), Guangdong Basic and Applied Basic Research Foundation
819 (grant number: 2024A1515030117), and the Innovation Capability Support Plan Project in Shaanxi
820 Province (grant number: 2024ZC-KJXX-038) to W.Z.

821

822 **References**

823 Abugessaisa I, Noguchi S, Hasegawa A, Kondo A, Kawaji H, Carninci P, Kasukawa T. 2019. refTSS: A
824 Reference Data Set for Human and Mouse Transcription Start Sites. *J Mol Biol* **431**: 2407-2422.
825 Andersson R, Sandelin A. 2020. Determinants of enhancer and promoter activities of regulatory elements.
826 *Nat Rev Genet* **21**: 71-87.
827 Bao W, Kojima KK, Kohany O. 2015. Repbase Update, a database of repetitive elements in eukaryotic
828 genomes. *Mob DNA* **6**: 11.
829 Barbosa-Morais NL, Irimia M, Pan Q, Xiong HY, Gueroussov S, Lee LJ, Slobodeniuc V, Kutter C, Watt S,
830 Colak R et al. 2012. The evolutionary landscape of alternative splicing in vertebrate species. *Science*
831 **338**: 1587-1593.
832 Bekpen C, Xie C, Tautz D. 2018. Dealing with the adaptive immune system during de novo evolution of
833 genes from intergenic sequences. *BMC Evol Biol* **18**: 121.
834 Benitiere F, Necsulea A, Duret L. 2024. Random genetic drift sets an upper limit on mRNA splicing
835 accuracy in metazoans. *Elife* **13**.
836 Bray NL, Pimentel H, Melsted P, Pachter L. 2016. Near-optimal probabilistic RNA-seq quantification. *Nat*
837 *Biotechnol* **34**: 525-527.

838 Byrne A, Cole C, Volden R, Vollmers C. 2019. Realizing the potential of full-length transcriptome
839 sequencing. *Philos Trans R Soc Lond B Biol Sci* **374**: 20190097.
840 Cartolano M, Huettel B, Hartwig B, Reinhardt R, Schneeberger K. 2016. cDNA Library Enrichment of Full
841 Length Transcripts for SMRT Long Read Sequencing. *PLoS One* **11**: e0157779.
842 Chang YF, Imam JS, Wilkinson MF. 2007. The nonsense-mediated decay RNA surveillance pathway. *Annu*
843 *Rev Biochem* **76**: 51-74.
844 Chen S, Zhou Y, Chen Y, Gu J. 2018. fastp: an ultra-fast all-in-one FASTQ preprocessor. *Bioinformatics*
845 **34**: i884-i890.
846 Danecek P, Auton A, Abecasis G, Albers CA, Banks E, DePristo MA, Handsaker RE, Lunter G, Marth GT,
847 Sherry ST et al. 2011. The variant call format and VCFtools. *Bioinformatics* **27**: 2156-2158.
848 Ding C, Yan X, Xu M, Zhou R, Zhao Y, Zhang D, Huang Z, Pan Z, Xiao P, Li H et al. 2022. Short-read
849 and long-read full-length transcriptome of mouse neural stem cells across neurodevelopmental
850 stages. *Sci Data* **9**: 69.
851 Dobin A, Davis CA, Schlesinger F, Drenkow J, Zaleski C, Jha S, Batut P, Chaisson M, Gingeras TR. 2013.
852 STAR: ultrafast universal RNA-seq aligner. *Bioinformatics* **29**: 15-21.
853 Eisenberg E, Levanon EY. 2003. Human housekeeping genes are compact. *Trends Genet* **19**: 362-365.
854 Ferrandez-Peral L, Zhan X, Alvarez-Estape M, Chiva C, Esteller-Cucala P, Garcia-Perez R, Julia E, Lizano
855 E, Fornas O, Sabido E et al. 2022. Transcriptome innovations in primates revealed by single-
856 molecule long-read sequencing. *Genome Res* doi:10.1101/gr.276395.121.
857 Gordon SP, Tseng E, Salamov A, Zhang J, Meng X, Zhao Z, Kang D, Underwood J, Grigoriev IV, Figueroa
858 M et al. 2015. Widespread Polycistronic Transcripts in Fungi Revealed by Single-Molecule mRNA
859 Sequencing. *PLoS One* **10**: e0132628.
860 Grau-Bove X, Ruiz-Trillo I, Irimia M. 2018. Origin of exon skipping-rich transcriptomes in animals driven
861 by evolution of gene architecture. *Genome Biol* **19**: 135.
862 Gruber AR, Lorenz R, Bernhart SH, Neubock R, Hofacker IL. 2008. The Vienna RNA websuite. *Nucleic*
863 *Acids Res* **36**: W70-74.
864 Guenet JL, Bonhomme F. 2003. Wild mice: an ever-increasing contribution to a popular mammalian model.
865 *Trends Genet* **19**: 24-31.
866 Gupta I, Collier PG, Haase B, Mahfouz A, Joglekar A, Floyd T, Koopmans F, Barres B, Smit AB, Sloan
867 SA et al. 2018. Single-cell isoform RNA sequencing characterizes isoforms in thousands of
868 cerebellar cells. *Nat Biotechnol* doi:10.1038/nbt.4259.
869 Harr B, Karakoc E, Neme R, Teschke M, Pfeifle C, Pezer Z, Babiker H, Linnenbrink M, Montero I, Scavetta
870 R et al. 2016. Genomic resources for wild populations of the house mouse, Mus musculus and its
871 close relative Mus spretus. *Sci Data* **3**: 160075.
872 Harr B, Turner LM. 2010. Genome-wide analysis of alternative splicing evolution among Mus subspecies.
873 *Mol Ecol* **19 Suppl 1**: 228-239.
874 Herrmann CJ, Schmidt R, Kanitz A, Artimo P, Gruber AJ, Zavolan M. 2020. PolyASite 2.0: a consolidated
875 atlas of polyadenylation sites from 3' end sequencing. *Nucleic Acids Res* **48**: D174-D179.
876 Howe KL, Achuthan P, Allen J, Allen J, Alvarez-Jarreta J, Amode MR, Armean IM, Azov AG, Bennett R,
877 Bhai J et al. 2021. Ensembl 2021. *Nucleic Acids Res* **49**: D884-D891.
878 Huang KK, Huang J, Wu JKL, Lee M, Tay ST, Kumar V, Ramnarayanan K, Padmanabhan N, Xu C, Tan
879 ALK et al. 2021. Long-read transcriptome sequencing reveals abundant promoter diversity in
880 distinct molecular subtypes of gastric cancer. *Genome Biol* **22**: 44.
881 Ilik IA, Glazar P, Tse K, Brandl B, Meierhofer D, Muller FJ, Smith ZD, Aktas T. 2024. Autonomous
882 transposons tune their sequences to ensure somatic suppression. *Nature* doi:10.1038/s41586-024-
883 07081-0.
884 Joglekar A, Prjibelski A, Mahfouz A, Collier P, Lin S, Schlusche AK, Marrocco J, Williams SR, Haase B,
885 Hayes A et al. 2021. A spatially resolved brain region- and cell type-specific isoform atlas of the
886 postnatal mouse brain. *Nat Commun* **12**: 463.

887 Keren H, Lev-Maor G, Ast G. 2010. Alternative splicing and evolution: diversification, exon definition and
888 function. *Nat Rev Genet* **11**: 345-355.
889 Kuo RI, Cheng Y, Zhang R, Brown JWS, Smith J, Archibald AL, Burt DW. 2020. Illuminating the dark
890 side of the human transcriptome with long read transcript sequencing. *BMC Genomics* **21**: 751.
891 Kuo RI, Tseng E, Eory L, Paton IR, Archibald AL, Burt DW. 2017. Normalized long read RNA sequencing
892 in chicken reveals transcriptome complexity similar to human. *BMC Genomics* **18**: 323.
893 Landry JR, Mager DL, Wilhelm BT. 2003. Complex controls: the role of alternative promoters in
894 mammalian genomes. *Trends Genet* **19**: 640-648.
895 Lebrigand K, Magnone V, Barbry P, Waldmann R. 2020. High throughput error corrected Nanopore single
896 cell transcriptome sequencing. *Nat Commun* **11**: 4025.
897 Leong AZ, Lee PY, Mohtar MA, Syafruddin SE, Pung YF, Low TY. 2022. Short open reading frames
898 (sORFs) and microproteins: an update on their identification and validation measures. *J Biomed Sci*
899 **29**: 19.
900 Leung SK, Jeffries AR, Castanho I, Jordan BT, Moore K, Davies JP, Dempster EL, Bray NJ, O'Neill P,
901 Tseng E et al. 2021. Full-length transcript sequencing of human and mouse cerebral cortex identifies
902 widespread isoform diversity and alternative splicing. *Cell Rep* **37**: 110022.
903 Li H. 2018. Minimap2: pairwise alignment for nucleotide sequences. *Bioinformatics* **34**: 3094-3100.
904 Li H, Handsaker B, Wysoker A, Fennell T, Ruan J, Homer N, Marth G, Abecasis G, Durbin R, Genome
905 Project Data Processing S. 2009. The Sequence Alignment/Map format and SAMtools.
906 *Bioinformatics* **25**: 2078-2079.
907 Liao Y, Smyth GK, Shi W. 2014. featureCounts: an efficient general purpose program for assigning
908 sequence reads to genomic features. *Bioinformatics* **30**: 923-930.
909 Lin L, Shen S, Jiang P, Sato S, Davidson BL, Xing Y. 2010. Evolution of alternative splicing in primate
910 brain transcriptomes. *Hum Mol Genet* **19**: 2958-2973.
911 Lin S, Lin Y, Nery JR, Urich MA, Breschi A, Davis CA, Dobin A, Zaleski C, Beer MA, Chapman WC et
912 al. 2014. Comparison of the transcriptional landscapes between human and mouse tissues. *Proc*
913 *Natl Acad Sci U S A* **111**: 17224-17229.
914 Ling Z, Brockmoller T, Baldwin IT, Xu S. 2019. Evolution of Alternative Splicing in Eudicots. *Front Plant*
915 *Sci* **10**: 707.
916 Malko DB, Makeev VJ, Mironov AA, Gelfand MS. 2006. Evolution of exon-intron structure and alternative
917 splicing in fruit flies and malarial mosquito genomes. *Genome Res* **16**: 505-509.
918 Manichaikul A, Mychaleckyj JC, Rich SS, Daly K, Sale M, Chen WM. 2010. Robust relationship inference
919 in genome-wide association studies. *Bioinformatics* **26**: 2867-2873.
920 Mudge JM, Frankish A, Fernandez-Banet J, Alioto T, Derrien T, Howald C, Reymond A, Guigo R, Hubbard
921 T, Harrow J. 2011. The origins, evolution, and functional potential of alternative splicing in
922 vertebrates. *Mol Biol Evol* **28**: 2949-2959.
923 Murat F, Mbengue N, Winge SB, Trefzer T, Leushkin E, Sepp M, Cardoso-Moreira M, Schmidt J, Schneider
924 C, Mossinger K et al. 2023. The molecular evolution of spermatogenesis across mammals. *Nature*
925 **613**: 308-316.
926 Naftaly AS, Pau S, White MA. 2021. Long-read RNA sequencing reveals widespread sex-specific
927 alternative splicing in threespine stickleback fish. *Genome Res* **31**: 1486-1497.
928 Neme R, Tautz D. 2013. Phylogenetic patterns of emergence of new genes support a model of frequent de
929 novo evolution. *BMC Genomics* **14**: 117.
930 Neme R, Tautz D. 2016. Fast turnover of genome transcription across evolutionary time exposes entire non-
931 coding DNA to de novo gene emergence. *Elife* **5**.
932 Nilsen TW, Graveley BR. 2010. Expansion of the eukaryotic proteome by alternative splicing. *Nature* **463**:
933 457-463.
934 Parada GE, Munita R, Cerda CA, Gysling K. 2014. A comprehensive survey of non-canonical splice sites
935 in the human transcriptome. *Nucleic Acids Res* **42**: 10564-10578.

936 Paradis E, Schliep K. 2019. ape 5.0: an environment for modern phylogenetics and evolutionary analyses
937 in R. *Bioinformatics* **35**: 526-528.
938 Pertea G, Pertea M. 2020. GFF Utilities: GffRead and GffCompare. *F1000Res* **9**.
939 Pezer Z, Harr B, Teschke M, Babiker H, Tautz D. 2015. Divergence patterns of genic copy number variation
940 in natural populations of the house mouse (Mus musculus domesticus) reveal three conserved genes
941 with major population-specific expansions. *Genome Res* **25**: 1114-1124.
942 Phifer-Rixey M, Nachman MW. 2015. Insights into mammalian biology from the wild house mouse Mus
943 musculus. *Elife* **4**.
944 Pickrell JK, Pai AA, Gilad Y, Pritchard JK. 2010. Noisy splicing drives mRNA isoform diversity in human
945 cells. *PLoS Genet* **6**: e1001236.
946 Purcell S, Neale B, Todd-Brown K, Thomas L, Ferreira MA, Bender D, Maller J, Sklar P, de Bakker PI,
947 Daly MJ et al. 2007. PLINK: a tool set for whole-genome association and population-based linkage
948 analyses. *Am J Hum Genet* **81**: 559-575.
949 Rogers TF, Palmer DH, Wright AE. 2021. Sex-Specific Selection Drives the Evolution of Alternative
950 Splicing in Birds. *Mol Biol Evol* **38**: 519-530.
951 Saudemont B, Popa A, Parmley JL, Rocher V, Blugeon C, Necsulea A, Meyer E, Duret L. 2017. The fitness
952 cost of mis-splicing is the main determinant of alternative splicing patterns. *Genome Biol* **18**: 208.
953 Sharon D, Tilgner H, Grubert F, Snyder M. 2013. A single-molecule long-read survey of the human
954 transcriptome. *Nat Biotechnol* **31**: 1009-1014.
955 Staubach F, Lorenc A, Messer PW, Tang K, Petrov DA, Tautz D. 2012. Genome patterns of selection and
956 introgression of haplotypes in natural populations of the house mouse (Mus musculus). *PLoS Genet*
957 **8**: e1002891.
958 Tang S, Lomsadze A, Borodovsky M. 2015. Identification of protein coding regions in RNA transcripts.
959 *Nucleic Acids Res* **43**: e78.
960 Tardaguila M, de la Fuente L, Marti C, Pereira C, Pardo-Palacios FJ, Del Risco H, Ferrell M, Mellado M,
961 Macchietto M, Verheggen K et al. 2018. SQANTI: extensive characterization of long-read
962 transcript sequences for quality control in full-length transcriptome identification and quantification.
963 *Genome Res* doi:10.1101/gr.222976.117.
964 Team RC. 2022. R: A language and environment for statistical computing. *R Foundation for Statistical*
965 *Computing, Vienna, Austria*.
966 Tempel S. 2012. Using and understanding RepeatMasker. *Methods Mol Biol* **859**: 29-51.
967 Tian B, Manley JL. 2017. Alternative polyadenylation of mRNA precursors. *Nat Rev Mol Cell Biol* **18**: 18-
968 30.
969 Trincado JL, Entizne JC, Hysenaj G, Singh B, Skalic M, Elliott DJ, Eyras E. 2018. SUPPA2: fast, accurate,
970 and uncertainty-aware differential splicing analysis across multiple conditions. *Genome Biol* **19**: 40.
971 Verta JP, Jacobs A. 2022. The role of alternative splicing in adaptation and evolution. *Trends Ecol Evol* **37**:
972 299-308.
973 Wan Y, Larson DR. 2018. Splicing heterogeneity: separating signal from noise. *Genome Biol* **19**: 86.
974 Young MD, Wakefield MJ, Smyth GK, Oshlack A. 2010. Gene ontology analysis for RNA-seq: accounting
975 for selection bias. *Genome Biol* **11**: R14.
976 Zhang W, Landback P, Gschwend AR, Shen B, Long M. 2015. New genes drive the evolution of gene
977 interaction networks in the human and mouse genomes. *Genome Biol* **16**: 202.
978 Zhang W, Tautz D. 2022. Tracing the Origin and Evolutionary Fate of Recent Gene Retrocopies in Natural
979 Populations of the House Mouse. *Mol Biol Evol* **39**.
980 Zhang W, Xie C, Ullrich K, Zhang YE, Tautz D. 2021. The mutational load in natural populations is
981 significantly affected by high primary rates of retroposition. *Proc Natl Acad Sci U S A* **118**.

982

983

984

985 **Table 1 Statistics on the detected isoforms in the house mouse populations and outgroups.** The digit succeeding the character N indicates the number of
986 sequenced mouse individuals in each population. The graphic depiction of isoform categories is shown in Figure 4A. Isoforms categorized as FSM and ISM are defined
987 to be known isoforms, gene loci with any isoform not categorized as either Antisense or Intergenic to be annotated genes. SD values refer to variances between the
988 individuals in a given population.

	M. m. domesticus			*M. m. musculus*	*M. m. castaneus*	*M. spicilegus*	*M. spretus*
	GE (N: 8)	**FR (N: 8)**	**IR (N: 8)**	**KA (N: 8)**	**TA (N: 8)**	**SL (N: 4)**	**SP (N: 4)**
Unique isoforms	23,027 (SD:2,001)	21,609 (SD:2,315)	21,763 (SD:2,006)	22,380 (SD:1,553)	21,279 (SD:1,532)	20,644 (SD:858)	21,640 (SD:640)
Protein-coding	21,394 (SD:2,062)	20,024 (SD:2,431)	20,155 (SD:1,941)	20,798 (SD:1,486)	19,642 (SD:1,435)	18,786 (SD:929)	20,063 (SD:597)
Nonsense-mediated decay	1,152 (SD:226)	1,071 (SD: 220)	1,098 (SD:209)	1,125 (SD:146)	1,142 (SD:216)	1,038 (SD:146)	1,131 (SD:46)
Non-protein-coding	1,634 (SD:239)	1,585 (SD:284)	1,608 (SD:324)	1,582 (SD:235)	1,637 (SD:261)	1,858 (SD:73)	1,577 (SD:63)
Known isoforms	17,266 (SD:1,216)	16,306 (SD: 1,419)	16,343 (SD:1,257)	16,487 (SD:861)	15,765 (SD:821)	15,202 (SD:512)	15,608 (SD:416)
Full Splice Match (FSM)	15,007 (SD:1,217)	14,245 (SD: 1,441)	13,654 (SD:1,053)	14,466 (SD:810)	13,561 (SD:602)	12,812 (SD:523)	13,621 (SD:297)
Incomplete Splice Match (ISM)	2,259 (SD:297)	2,060 (SD: 654)	2,689 (SD:531)	2,021 (SD:593)	2,204 (SD:313)	2,389 (SD:325)	1,988 (SD:154)
Novel isoforms	5,762 (SD:796)	5,304 (SD: 913)	5,421 (SD:778)	5,893 (SD:708)	5,514 (SD:768)	5,442 (SD:415)	6,032 (SD:237)
Not In Category (NIC)	3,765 (SD:599)	3,490(SD:651)	3,478 (SD:514)	3,611 (SD:459)	3,469 (SD:528)	3,204 (SD:318)	3,582 (SD:165)
Novel Not in Category (NNC)	1,811 (SD:202)	1,647 (SD: 271)	1,768 (SD:256)	2,066 (SD:254)	1,839 (SD:234)	2,015 (SD:120)	2,248 (SD:59)
Fusion (F)	74 (SD:11)	67 (SD:15)	78 (SD:11)	90 (SD:18)	93(SD:17)	65 (SD:7)	84 (SD:8)
Genic (G)	22 (SD:5)	19 (SD:4)	18 (SD:5)	22 (SD:4)	25 (SD:4)	24 (SD:1)	24 (SD:3)
Antisense (A)	35 (SD:8)	30 (SD:10)	33 (SD:12)	32 (SD:6)	30 (SD:10)	49 (SD:12)	31 (SD:3)
Intergenic (I)	54 (SD:7)	51 (SD:13)	44 (SD:14)	72 (SD:10)	59 (SD:15)	84 (SD:6)	62 (SD:10)

989